Monatshefte für Chemie 135, 1335–1347 (2004)
DOI 10.1007/s00706-004-0209-3

Monatshefte für Chemie
Chemical Monthly
Printed in Austria

Synthesis, Structure, and Magnetic Properties of the Silicides *RE*IrSi (*RE* = Ce, Pr, Er, Tm, Lu) and $SmIr_{0.266(8)}Si_{1.734(8)}$

Birgit Heying[1], **Rainer Pöttgen**[1,*], **Martin Valldor**[1], **Ute Ch. Rodewald**[1], **Ratikanta Mishra**[2], and **Rolf-Dieter Hoffmann**[1]

[1] Institut für Anorganische und Analytische Chemie, Westfälische Wilhelms-Universität Münster, 48149 Münster, Germany
[2] Applied Chemistry Division, Bhabha Atomic Research Centre Trombay, Mumbai-400 085, India

Received March 12, 2004; accepted (revised) April 6, 2004
Published online August 16, 2004

Summary. The equiatomic rare earth metal–iridium–silicides *RE*IrSi (*RE* = Ce, Pr, Er, Tm, Lu) were prepared by arc-melting of the elements and subsequent annealing. All silicides were characterized through their X-ray powder patterns. The structures of CeIrSi, ErIrSi, and LuIrSi were refined from X-ray single crystal diffractometer data: LaIrSi type, $P2_13$, $a = 629.15(2)$ pm, $wR2 = 0.1232$, 280 F^2 values, and 11 variable parameters for CeIrSi; TiNiSi type, *Pnma*, $a = 673.4(1)$, $b = 416.07(5)$, $c = 744.88(9)$ pm, $wR2 = 0.0705$, 339 F^2 values, and 20 variable parameters for ErIrSi, and $a = 664.0(3)$, $b = 412.9(1)$, $c = 742.6(1)$ pm, $wR2 = 0.0398$, 496 F^2 values, and 20 variable parameters for LuIrSi. The iridium and silicon atoms in CeIrSi, ErIrSi, and LuIrSi build three-dimensional [IrSi] networks where the iridium atoms have three (CeIrSi, Ir–Si 229 pm) and four (ErIrSi, Ir–Si 247–258 pm; LuIrSi, Ir–Si 245–256 pm) silicon neighbors. The [IrSi] networks leave larger channels in which the cerium, erbium, and lutetium atoms are located. Temperature dependent susceptibility data for LuIrSi indicate *Pauli* paramagnetism. CeIrSi shows *Curie-Weiss* paramagnetism above 100 K with an experimental magnetic moment of 2.56(2) μ_B/Ce atom. With samarium as rare earth metal component the silicide $SmIr_{0.266(8)}Si_{1.734(8)}$ with α-$ThSi_2$ type structure was obtained: $I4_1/amd$, $a = 409.3(1)$, $c = 1397.2(5)$ pm, $wR2 = 0.0575$, 161 F^2 values, and 9 variable parameters. Within the three-dimensional $[Ir_{0.266}Si_{1.734}]$ network the Ir/Si–Ir/Si distances range from 230 to 237 pm.

Keywords. Rare earth compounds; Crystal chemistry; Magnetochemistry.

* Corresponding author. E-mail: pottgen@uni-muenster.de

Introduction

The ternary systems rare earth metal (*RE*)–transition metal–silicon (germanium) have intensively been investigated in the past 30 years with respect to phase analyses, crystal structures, and their greatly varying magnetic and electrical properties [1–5]. Generally such silicides or germanides are readily available *via* arc-melting of the elements. This synthesis technique is difficult or even not suitable when the transition metal has a comparatively high vapor pressure at the syntheses temperatures. Such problems occur with manganese, zinc, and silver. Another difficulty are the very high melting temperatures of osmium (3327 K) and iridium (2683 K) [6]. Sometimes the reactions are not complete and some residual iridium or osmium remains in the samples. This might be one of the reasons, why the series of rare earth-transition metal-silicides and germanides are sometimes incomplete.

In the series of *RE*IrSi silicides only those with *RE* = Sc, Y, La, Nd, Gd, Tb, Dy, Ho, Er, and Yb have been reported [7–14]. LaIrSi crystallizes with its own cubic structure type [8] and adopts a ternary ordered version of the $SrSi_2$ type, as NdIrSi does. The other *RE*IrSi silicides crystallize with the well known orthorhombic TiNiSi type. Several of these silicides have been studied with respect to their magnetic and electrical properties. YIrSi [10] and LaIrSi [9] show transitions to the superconducting state at 2.7 and 2.3 K, respectively. NdIrSi orders ferromagnetically at $T_C = 10$ K [9], while TbIrSi, DyIrSi, HoIrSi, and ErIrSi order antiferromagnetically at *Néel* temperatures of 32, 7, 4.8, and 3.8 K, respectively [12, 14], in agreement with the *de Gennes* function. The complex magnetic structures have been determined from neutron powder diffraction data. The valence state of gadolinium in GdIrSi was studied through X-ray L_{III} absorption spectra [11].

Herein we report on the synthesis and structural investigation of the remaining compounds in the *RE*IrSi series. Additionally we determined the magnetic properties of CeIrSi and LuIrSi.

Results and Discussion

The *RE*IrSi silicides crystallize with two different structure types. With the larger rare earth elements La, Ce, Pr, and Nd they adopt the cubic LaIrSi type [8], space group $P2_13$, while those with the smaller rare earth elements crystallize with the orthorhombic TiNiSi type [28], space group *Pnma*. Both structure types have four formula units per cell. The course of the cell volumes of the *RE*IrSi silicides is shown in Fig. 1. As expected from the lanthanoid contraction, the cell volumes decrease from the lanthanum to the lutetium compound. The cell volume of YIrSi

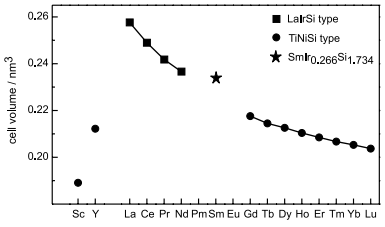

Fig. 1. Plot of the cell volumes of the *RE*IrSi silicides

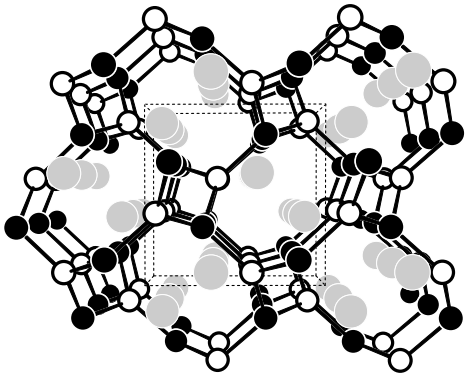

Fig. 2. Perspective view of the cubic CeIrSi structure; the cerium, iridium, and silicon atoms are drawn as light-gray, filled, and open circles, respectively; the three-dimensional [IrSi] network is emphasized

fits between that of DyIrSi and HoIrSi. The by far smallest cell volume occurs for ScIrSi. Even smaller are the cell volumes of the isotypic transition metal silicides NbIrSi (0.1771 nm^3) and TaIrSi (0.1756 nm^3) [29]. The change in the cell volumes is much more pronounced in the series of cubic *RE*IrSi than in the series of orthorhombic *RE*IrSi silicides. At this point it is worthwhile to note that the structures of the missing representatives of the *RE*IrSi series have already been predicted by *Hovestreydt* in 1988 [30].

A perspective view of the CeIrSi structure is shown in Fig. 2. The iridium and silicon atoms build up a three-dimensional [IrSi] network, where each iridium atom is connected to three silicon atoms at an Ir–Si distance of 229 pm, and *vice versa*. These Ir–Si distances are significantly smaller than the sum of the covalent radii of 243 pm [6]. Also in the structures of NbIrSi and TaIrSi (240–245 pm) [29], α-$CeIr_2Si_2$ (241 pm) [31], and $Er_4Ir_{13}Si_9$ (233–257 pm) [32], similar Ir–Si distances occur. We can thus assume strong covalent Ir–Si bonding in the CeIrSi structure. The bonding of the cerium atoms to the three-dimensional [IrSi] network, on the other hand, seems to be much weaker. The Ce–Ir (312 and 316 pm) and Ce–Si (317–357 pm) distances are longer than the sums of the covalent radii of 291 pm (Ce + Ir) and 282 pm (Ce + Si) [6]. Also the Ce–Ce distances of 386 pm are somewhat longer than in *fcc* cerium (365 pm) [33].

The *RE*IrSi silicides with the heavy rare earth elements adopt the orthorhombic TiNiSi type structure. As an example we present a drawing of the ErIrSi structure in Fig. 3. Each iridium atom has four silicon neighbors in a distorted tetrahedral coordination at Ir–Si distances between 247 and 258 pm, significantly longer than in the CeIrSi structure. The distorted $IrSi_{4/4}$ tetrahedra are condensed *via* all corners forming the three-dimensional [IrSi] network in which the erbium atoms are located in channels.

So far we got no equiatomic silicide with samarium and europium as rare earth metal component. The X-ray powder patterns of our samples with the starting compositions 1:1:1 revealed the tetragonal $REIr_2Si_2$ silicides as the main products. With samarium we identified the new silicide $SmIr_{0.266(8)}Si_{1.734(8)}$ with α-$ThSi_2$ structure (Fig. 4). The iridium and silicon atoms are randomly distributed on the 8*e*

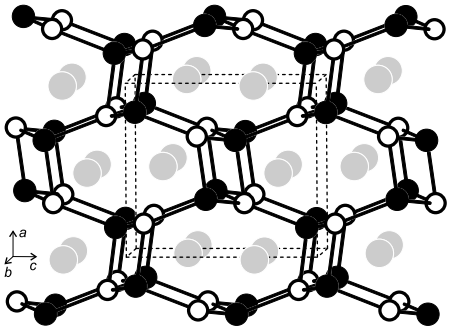

Fig. 3. View of the ErIrSi structure approximately along the *b* axis; the erbium, iridium, and silicon atoms are drawn as light-gray, filled, and open circles, respectively; the three-dimensional [IrSi] network is emphasized

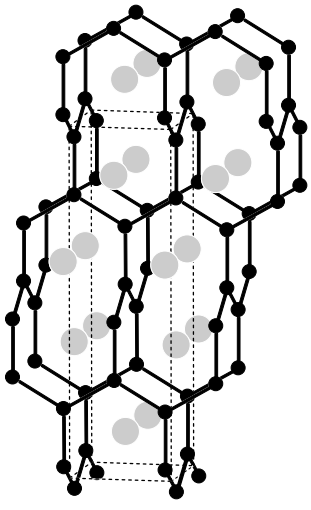

Fig. 4. View of the tetragonal $SmIr_{0.266}Si_{1.734}$ structure approximately along the *a* axis; the samarium and iridium/silicon atoms are drawn as light-gray and filled circles; the three-dimensional $[Ir_{0.266}Si_{1.734}]$ network is emphasized

position. An ordering of these atoms is only possible in a 1:1 ratio as it is realized for LaPtSi [34]. Each Ir/Si atom has a nearly regular, trigonal planar coordination within the three-dimensional $[Ir_{0.266(8)}Si_{1.734(8)}]$ network at Ir/Si–Ir/Si distances from 230 to 237 pm. Also these Ir–Si interactions can be considered as strong and the samarium atoms located within the network show weaker bonding. This situation is similar to the structures of CeIrSi and ErIrSi discussed above.

The partial substitution of silicon in $SmSi_2$ ($a = 404.9$, $c = 1336$ pm [35]) has a drastic effect on the lattice parameters. For the investigated sample with the refined composition $SmIr_{0.266(8)}Si_{1.734(8)}$ we find an expansion of the lattice parameters to $a = 409.3(1)$ and $c = 1397.2(5)$ pm. The increase of the *c* lattice parameter is much stronger (4.6%) than for the *a* parameter (1.1%), similar to the series of Th_2TSi_3 silicides [36]. Usually the ternary silicides with α-$ThSi_2$ structure show extended homogeneity ranges. We did not investigate the $SmIr_xSi_{2-x}$ system in detail, but our samples gave no hint for an equiatomic silicide.

For comparison we plotted also the cell volume of $SmIr_{0.266(8)}Si_{1.734(8)}$ in Fig. 1. The cell volume is slightly larger than that expected for an equiatomic silicide. This is certainly due to the statistical occupancy of the 8*e* site and the different coordination spheres of the samarium atoms, as compared to the LaIrSi and TiNiSi type structures.

Experimental

Synthesis

Starting materials for the preparation of the *RE*IrSi silicides were ingots of the rare earth metals (Johnson Matthey, Chempur or Kelpin), iridium powder (Degussa-Hüls, *ca.* 200 mesh), and silicon lumps, all with stated purities better than 99.9%. The rare earth ingots were first cut into smaller pieces and arc-melted [15] under argon to small buttons. The argon was purified over titanium sponge (900 K), silica gel, and molecular sieves. This pre-melting procedure strongly reduces shattering of the reaction mixture during the strongly exothermic reactions. The arc-melted rare earth metal buttons, cold-pressed pellets of iridium (Ø 6 mm), and pieces of the silicon lumps were then weighed in the ideal 1:1:1 atomic ratios and arc-melted under an argon pressure of about 800 mbar. The pellets were flipped over and re-melted three times to ensure homogeneity. The weight losses after the melting procedures were always smaller than 0.5 weight-%.

An alternative synthesis was performed for ErIrSi. The elements were sealed in a small tantalum tube (*ca.* 1 cm^3 volume) [15] under an atmosphere of *ca.* 800 mbar argon. The tube was placed in a water-cooled sample chamber of an induction furnace (Hüttinger Elektronik, Freiburg, Typ TIG 2.5/300), first heated for 10 minutes at white heat and subsequently annealed for another 2 hours at *ca.* 1500 K. Finally the tube was quenched to room temperature by switching off the power of the generator. The brittle product could readily be separated from the tube. No reaction with the container material could be observed. Small single crystals were available directly after this annealing procedure.

For crystal growth, the arc-melted CeIrSi sample was sealed in a silica tube and placed in a special water-cooled sample chamber [16] of a high-frequency furnace (Hüttinger Elektronik, Freiburg, Typ IG 10/600). The sample was annealed for 8 hours *ca.* 100 K below the (not determined) melting point. Due to the efficient water-cooling, no reaction of the silicide with the quartz ampoule was observed.

All *RE*IrSi samples are very brittle and can easily be fragmented in a steel mortar. Compact pieces and powders are stable in air over years. Powders are dark gray; single crystals exhibit metallic luster.

Scanning Electron Microscopy

The CeIrSi single crystal investigated on the diffractometer and the CeIrSi bulk sample were analyzed by EDX measurements using a LEICA 420 I scanning electron microscope with CeO_2, iridium, and SiO_2 as standards. The bulk sample was previously embedded in a metacrylate matrix and the surface was polished with a diamond paste. The surface remained unetched for the EDX measurements. No impurity elements were detected. Various point analyses revealed the compositions 35 ± 2 at.-% Ce: 34 ± 2 at.-% Ir: 31 ± 2 at.-% Si, close to the calculated composition 33.3 at.-% Ce: 33.3 at.-% Ir: 33.3 at.-% Si for CeIrSi. Analyses of the $SmIr_{0.266}Si_{1.734}$ and the LuIrSi crystals revealed the compositions 30 ± 2 at.-% Sm: 10 ± 2 at.-% Ir: 60 ± 2 at.-% Si and 34 ± 2 at.-% Lu: 36 ± 2 at.-% Ir: 30 ± 2 at.-% Si, close to the calculated compositions 33.3 at.-% Sm: 8.9 at.-% Ir: 57.8 at.-% Si and 33.3 at.-% Lu: 33.3 at.-% Ir: 33.3 at.-% Si. SmF_3 and LuF_3 were used as standards for these measurements.

X-Ray Film Data and Structure Refinements

All samples were characterized through their *Guinier* powder patterns using Cu Kα_1 radiation and α-quartz ($a = 491.30$, $c = 540.46$ pm) as an internal standard. The *Guinier* camera was equipped with an

Table 1. Lattice parameters of cubic (LaIrSi type, $P2_13$), tetragonal (α-$ThSi_2$ type, $I4_1/amd$), or orthorhombic (TiNiSi type, *Pnma*) *RE*IrSi compounds

Compound	a/pm	b/pm	c/pm	V/nm^3	Ref.
ScIrSi	641.8(1)	403.6(1)	729.9(2)	0.1891	[7]
YIrSi	678.9	418.8	746.2	0.2122	[10]
YIrSi	678.9(4)	418.8(2)	746.2(6)	0.2122	[7]
LaIrSi	636.3(3)	–	–	0.2576	[8]
LaIrSi	633.7(2)	–	–	0.2545	[9]
CeIrSi	629.15(2)	–	–	0.2490	this work
PrIrSi	623.0(1)	–	–	0.2418	this work
NdIrSi	618.5(2)	–	–	0.2366	[9]
NdIrSi	620.8(1)	–	–	0.2392	this work
$SmIr_{0.266}Si_{1.734}$	409.3(1)	–	1397.2(5)	0.2341	this work
GdIrSi	691.3(6)	423.5(4)	743.4(7)	0.2176	[7]
TbIrSi	686.18(4)	421.00(5)	742.62(6)	0.2145	[14]
TbIrSi	683.9(9)	420.2(5)	742.0(1)	0.2132	this work
DyIrSi	681.67(6)	419.29(5)	743.84(6)	0.2126	[14]
HoIrSi	677.03(7)	417.48(5)	744.32(9)	0.2104	[14]
HoIrSi	677.1(1)	417.37(6)	745.1(1)	0.2106	[13]
ErIrSi	670.1(9)	417.4(3)	746.7(5)	0.2089	[7]
ErIrSi	673.48(7)	415.94(5)	744.44(7)	0.2085	[14]
ErIrSi	673.4(1)	416.07(5)	744.88(9)	0.2087	this work
TmIrSi	669.6(1)	414.9(1)	744.0(1)	0.2067	this work
YbIrSi	667.2(2)	414.16(8)	742.8(2)	0.2053	[13]
LuIrSi	664.0(3)	412.9(1)	742.6(1)	0.2036	this work

imaging plate system (Fujifilm BAS–1800). The lattice parameters (Table 1) were obtained from least-squares fits of the *Guinier* data. To ensure correct indexing, the observed patterns were compared to calculated ones [17] using the atomic positions obtained from the structure refinements. The lattice parameters derived for the powders and the single crystals agreed well. For NdIrSi, TbIrSi, and ErIrSi our lattice parameters show good agreement with the literature data (Table 1).

Irregularly shaped single crystals of CeIrSi, $SmIr_{0.266}Si_{1.734}$, ErIrSi, and LuIrSi were isolated from the annealed samples by mechanical fragmentation and first examined by *Laue* photographs on a *Buerger* precession camera (equipped with an imaging plate system Fujifilm BAS-1800) in order to establish suitability for intensity data collection. Intensity data of CeIrSi were recorded at room temperature by use of a Stoe IPDS-II diffractometer with graphite monochromatized Mo Kα radiation. The absorption correction for this crystal was numerical (X-Shape/X-Red). The data sets for $SmIr_{0.266}Si_{1.734}$, ErIrSi, and LuIrSi were collected at room temperature by use of a four-circle diffractometer (CAD4) with graphite monochromatized Mo Kα ($\lambda = 71.073$ pm) radiation and a scintillation counter with pulse height discrimination. The scans were taken in the $\omega/2\theta$ mode and empirical absorption corrections were applied on the basis of psi-scan data. All relevant crystallographic data and details for the data collections and evaluations are listed in Table 2.

The isotypy of CeIrSi, ErIrSi, and LuIrSi with the previously reported silicides LaIrSi [8] and HoIrSi [13] was already evident from the X-ray powder data. The atomic positions of these silicides were taken as starting values. The starting positional parameters for $SmIr_{0.266}Si_{1.734}$ were deduced from an automatic interpretation of direct methods with SHELXS-97 [18]. The four structures were then successfully refined using SHELXL-97 (full-matrix least-squares on F_o^2 [19] with anisotropic atomic displacement parameters for all sites.

Table 2. Crystal data and structure refinement for CeIrSi, $SmIr_{0.266}Si_{1.734}$, ErIrSi, and LuIrSi

Empirical formula	CeIrSi	$SmIr_{0.266}Si_{1.734}$
Formula weight/g mol^{-1}	360.41	250.02
Unit cell dimensions	Table 1	Table 1
Pearson symbol	c*P*12	t*P*12
Structure type	LaIrSi	α-$ThSi_2$
Space group	$P2_13$	$I4_1/amd$
Formula units per cell	$Z=4$	$Z=4$
Calculated density/g cm^{-3}	9.61	7.10
Crystal size/μm^3	5×60×100	10×40×40
Diffractometer type	Stoe IPDS-II	CAD4
Transmission ratio (max/min)	1.74	1.49
Absorption coefficient/mm^{-1}	71.5	40.5
F(000)	596	427
Detector distance/mm	60	–
Exposure time/min	20	–
ω range/°; increment/°	0–180, 1.0	–
Integr. parameters A, B, EMS	10.0, 1.5, 0.01	–
θ range for data collection/°	4 to 32	5 to 35
Range in *hkl*	$\pm9, -9\leq k\leq 8, \pm9$	$\pm6, \pm6, +22$
Total no. of reflections	2890	965
Independent reflections	280 ($R_{int}=0.1021$)	161 ($R_{int}=0.1191$)
Reflections with $I>2\sigma(I)$	256 ($R_{sigma}=0.0392$)	128 ($R_{sigma}=0.0615$)
Flack parameter	−0.01(6)	–
Data/parameters	280/11	161/9
Goodness-of-fit on F^2	1.099	1.073
Final R indices [$I>2\sigma(I)$]	$R1=0.0507$	$R1=0.0350$
	$wR2=0.1186$	$wR2=0.0528$
R indices (all data)	$R1=0.0576$	$R1=0.0581$
	$wR2=0.1232$	$wR2=0.0575$
Extinction coefficient	0.008(2)	0.005(1)
Largest diff. peak and hole/e Å^{-3}	6.33 and −4.94	1.74 and −2.47
Empirical formula	ErIrSi	LuIrSi
Formula weight/g mol^{-1}	387.55	395.26
Unit cell dimensions	Table 1	Table 1
Pearson symbol	o*P*12	o*P*12
Structure type	TiNiSi	TiNiSi
Space group	*Pnma*	*Pnma*
Formula units per cell	$Z=4$	$Z=4$
Calculated density/g cm^{-3}	12.33	12.90
Crystal size/μm^3	10×30×40	20×40×40
Diffractometer type	CAD4	CAD4
Transmission ratio (max/min)	3.09	1.95
Absorption coefficient/mm^{-1}	103.7	113.6
F(000)	636	648
θ range for data collection/°	4 to 30	4 to 35
Range in *hkl*	$\pm9, +5, \pm10$	$\pm10, +6, \pm11$
Total no. of reflections	1237	1857

(*continued*)

Table 2 (*continued*)

Independent reflections	339 ($R_{int} = 0.0830$)	496 ($R_{int} = 0.0586$)
Reflections with $I > 2\sigma(I)$	289 ($R_{sigma} = 0.0515$)	388 ($R_{sigma} = 0.0410$)
Data/parameters	339/20	496/20
Goodness-of-fit on F^2	1.088	1.049
Final R indices [$I > 2\sigma(I)$]	$R1 = 0.0317$	$R1 = 0.0240$
	$wR2 = 0.0684$	$wR2 = 0.0370$
R indices (all data)	$R1 = 0.0401$	$R1 = 0.0404$
	$wR2 = 0.0705$	$wR2 = 0.0398$
Extinction coefficient	0.0052(6)	0.0035(2)
Largest diff. peak and hole/e Å^{-3}	3.78 and −5.04	2.88 and −2.72

As a check for the correct composition, the occupancy parameters were refined in a separate series of least-squares cycles. The sites are fully occupied within two standard deviations for CeIrSi, ErIrSi, and LuIrSi. In the last cycles, the ideal occupancies were assumed again. For the $SmIr_{0.266(8)}Si_{1.734(8)}$ crystal the 8*e* site was refined with a mixed Ir/Si occupancy. Refinement of the correct absolute structure of the CeIrSi crystal was ensured through refinement of the *Flack* parameter [20, 21]. Final difference *Fourier* synthesis revealed no significant residual peaks (see Table 2). The highest residual peaks were close to the iridium sites and most likely resulted from incomplete absorption corrections of these strongly absorbing compounds, especially for the CeIrSi crystal. The positional parameters and interatomic distances are listed in Tables 3 and 4. Listings of the observed and calculated structure factors are available at Fachinformationszentrum Karlsruhe, D-76344 Eggenstein-Leopoldshafen

Table 3. Atomic coordinates and isotropic displacement parameters (pm^2) for CeIrSi, $SmIr_{0.266}Si_{1.734}$, ErIrSi, and LuIrSi; U_{eq} is defined as one third on the trace of the orthogonalized U_{ij} tensor

Atom	*Wyckoff* position	x	y	z	U_{eq}
CeIrSi (space group $P2_13$)					
Ce	4*a*	0.6183(2)	x	x	100(5)
Ir	4*a*	0.3282(2)	x	x	224(6)
Si	4*a*	0.909(1)	x	x	218(25)
$SmIr_{0.266}Si_{1.734}$ (space group $I4_1/amd$)					
Sm	4*b*	1/2	1/4	1/8	62(3)
Ir/Si[a]	8*e*	0	1/4	0.9574(1)	94(7)
ErIrSi (space group *Pnma*)					
Er	4*c*	0.9936(1)	1/4	0.6864(1)	95(3)
Ir	4*c*	0.3431(1)	1/4	0.43600(8)	91(2)
Si	4*c*	0.2053(8)	1/4	0.1129(7)	102(9)
LuIrSi (space group *Pnma*)					
Lu	4*c*	0.99114(7)	1/4	0.68640(7)	39(1)
Ir	4*c*	0.34135(7)	1/4	0.43765(5)	32(1)
Si	4*c*	0.2060(5)	1/4	0.1151(4)	42(5)

[a] This site is occupied by 13.3(4)% Ir and 86.7(4)% Si

Table 4. Interatomic distances (pm) in the structures of CeIrSi, $SmIr_{0.266}Si_{1.734}$, ErIrSi, and LuIrSi calculated with the lattice parameters obtained from the *Guinier* powder data; all distances within the first coordination sphere are listed

CeIrSi				$SmIr_{0.266}Si_{1.734}$				ErIrSi				LuIrSi			
Ce:	3	Ir	312.2(1)	Sm:	4	Ir/Si	311.0(2)	Er:	2	Si	289.1(4)	Lu:	2	Si	285.5(2)
	1	Ir	316.2(3)		8	Ir/Si	311.5(1)		2	Si	295.6(4)		2	Si	293.1(3)
	1	Si	317(1)		4	Sm	404.8(1)		1	Si	295.7(6)		1	Si	293.2(3)
	3	Si	326(1)		4	Sm	409.3(1)		1	Ir	299.0(3)		1	Ir	296.4(1)
	3	Si	357.3(6)	Ir/Si:	1	Ir/Si	230.3(4)		2	Ir	299.9(2)		1	Ir	297.0(1)
	3	Ir	374.0(2)		2	Ir/Si	236.7(2)		1	Ir	300.3(2)		2	Ir	299.7(1)
	6	Ce	385.5(1)		2	Sm	311.0(2)		2	Ir	320.9(2)		2	Ir	316.0(1)
Ir:	3	Si	228.5(1)		4	Sm	311.5(1)		2	Er	347.1(3)		2	Lu	345.2(2)
	3	Ce	312.2(1)						1	Si	348.2(6)		2	Lu	345.5(1)
	1	Ce	316.2(3)						2	Er	349.8(1)		1	Si	348.8(3)
	3	Ce	374.0(2)					Ir:	1	Si	246.7(5)	Ir:	1	Si	245.3(4)
Si:	3	Ir	228.5(1)						2	Si	248.4(4)		2	Si	246.9(2)
	1	Ce	317(1)						1	Si	257.9(6)		1	Si	255.9(3)
	3	Ce	326(1)						1	Er	299.0(3)		1	Lu	296.4(1)
	3	Ce	357.3(6)						2	Er	299.9(2)		1	Lu	297.0(1)
									1	Er	300.3(2)		2	Lu	299.7(1)
									2	Ir	311.5(2)		2	Ir	309.2(1)
									2	Er	320.9(2)		2	Lu	316.0(1)
								Si:	1	Ir	246.7(5)	Si:	1	Ir	245.3(4)
									2	Ir	248.4(4)		2	Ir	246.9(2)
									1	Ir	257.9(6)		1	Ir	255.9(3)
									2	Er	289.1(4)		2	Lu	285.5(2)
									2	Er	295.6(4)		2	Lu	293.1(3)
									1	Er	295.7(6)		1	Lu	293.2(3)
									1	Er	348.2(6)		1	Lu	348.8(3)

(Germany), by quoting the Registry No's. CSD–413854 (CeIrSi), CSD-413855 ($SmIr_{0.266}Si_{1.734}$), CSD-413856 (ErIrSi), and CSD-413857 (LuIrSi).

Rietveld Data of CeIrSi

The bulk sample of CeIrSi has also been studied on a powder diffractometer (Stoe Stadi P, Cu Kα_1 radiation) in order to perform a full profile *Rietveld* refinement. The measurement was performed in *Debye-Scherrer* geometry using Cu Kα_1 radiation ($\lambda = 154.0598$ pm, Ge monochromator) within the 2θ range 12–100° in steps of 0.02° (2θ).

The *Rietveld* calculations for the CeIrSi data set were performed with the FULLPROF [22] software. The background was set manually and the profiles were modelled using the pseudo-*Voigt* function (No. 5). The limit of peak asymmetry was set to 60 degrees (2θ) and an arbitrary absorption value of $\mu R = 1.4$ was used. 68 reflections could be observed, to which 15 parameters were fitted: 3 fractional coordinates, 3 isotropic displacement parameters, the scale factor, 1 cell parameter, the zero-position, 4 peak profile parameters, and 2 peak asymmetry parameters. The standard deviations of the refined parameters have been multiplied with the *Bérar-Lelann* factor [23]. The refinement smoothly converged to the residuals $R_{Bragg} = 0.0749$, $R_F = 0.0522$, and a goodness-of-fit of 1.40. The resulting

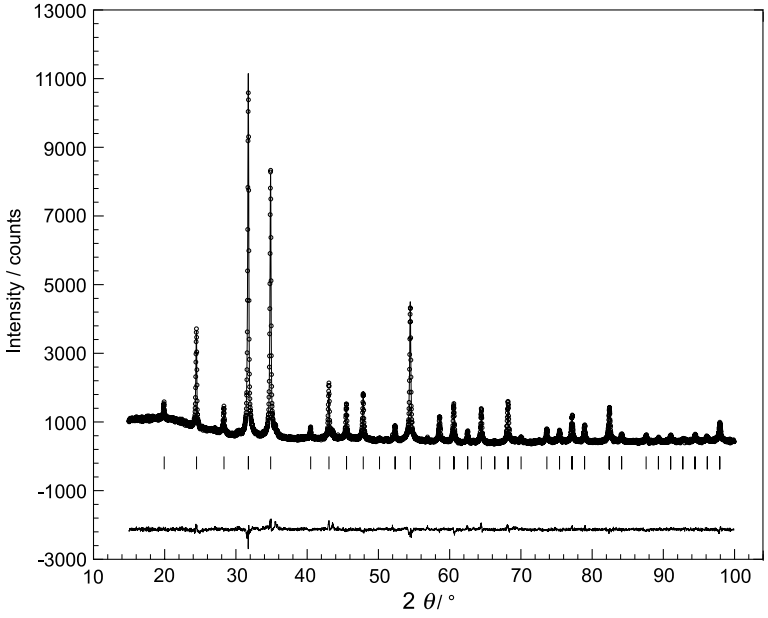

Fig. 5. *Rietveld* refinement plot for CeIrSi, in which the observed intensities are indicated with open circles and the calculated pattern with a line on top of the circles; the vertical lines indicate the *Bragg* positions; the difference y(obs)–y(calc) is drawn below the *Bragg* indicators

positional x parameters for the cerium (0.6170(7)), iridium (0.3300(5)), and silicon (0.908(3)) atoms agree well with the single crystal data, however, with larger standard deviations. The plot of the experimental and calculated intensity data is presented in Fig. 5.

Magnetic Data of CeIrSi and LuIrSi

The magnetic susceptibilities of polycrystalline, powdered samples of CeIrSi and LuIrSi were determined with a Quantum Design PPMS in the temperature range 2 to 300 K with magnetic flux densities up to 9 T. Quantities of 109.4 mg (CeIrSi) and 232.65 mg (LuIrSi) were enclosed in small gelatin capsules and fixed at the sample holder rod. The samples were then cooled to 2 K in zero magnetic field and slowly heated to room temperature in an applied external field.

The susceptibility of LuIrSi (2 T data) is almost independent of temperatures above 80 K, indicating *Pauli* paramagnetism (Fig. 6). At room temperature the susceptibility has a value of $53(1) \cdot 10^{-6}\,\mathrm{cm}^3/\mathrm{mol}$. The upturn below 80 K may be attributed to minor amounts of paramagnetic impurities, although the *Guinier* pattern showed only the reflections of LuIrSi.

The temperature dependence of the reciprocal magnetic susceptibility of CeIrSi measured at 1 T is presented in Fig. 7. Above 100 K CeIrSi obeys the *Curie-Weiss* law with an experimental magnetic moment of 2.56(2) μ_B/Ce atom and a paramagnetic *Curie* temperature (*Weiss* constant) of $-24(1)$ K. The experimental moment is close to the value of 2.54 μ_B for the free Ce^{3+} ion [24]. Below 50 K the inverse susceptibility significantly deviates from *Curie-Weiss* behavior, indicating crystal field splitting of the $J = 5/2$ ground state of the Ce^{3+} ions, but also the beginning of short range magnetic fluctuations. Similar behavior was recently also observed for $Ce_2Au_3In_5$ [25], $Ce_3Pd_4Sn_6$ [26], and CeAgMg [27]. The magnetization behavior is presented in Fig. 8. At 100 K we observe a linear increase with very small magnetic moments as expected for a paramagnetic material. At 2 K the magnetization curve shows a stronger increase and a tendency for saturation. The magnetic moment at the highest obtainable field of 9 T is 0.87(1) μ_B/Ce atom, much smaller than the maximum possible value of 2.14 μ_B/Ce atom [24]. The external field forces the cerium magnetic moments towards a parallel spin alignment.

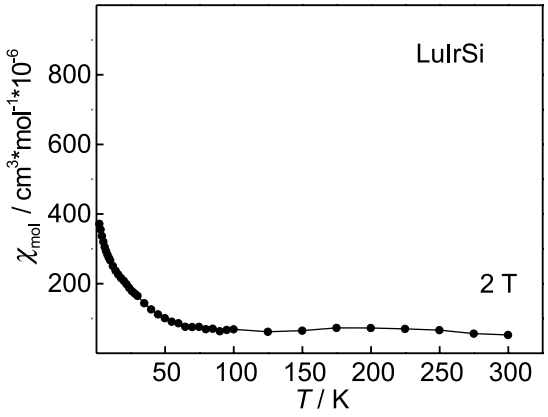

Fig. 6. Temperature dependence of the magnetic susceptibility of LuIrSi measured at a flux density of 2 T

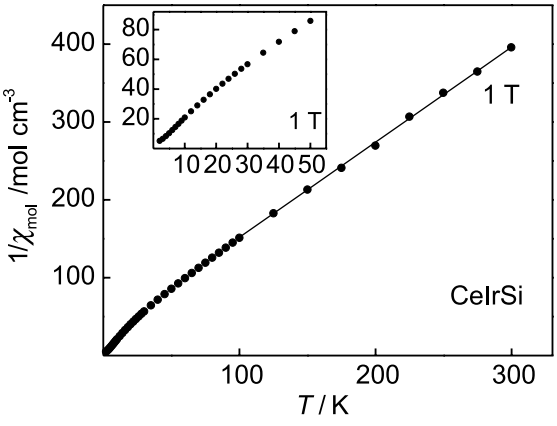

Fig. 7. Temperature dependence of the reciprocal magnetic susceptibility of CeIrSi measured at a flux density of 1 T

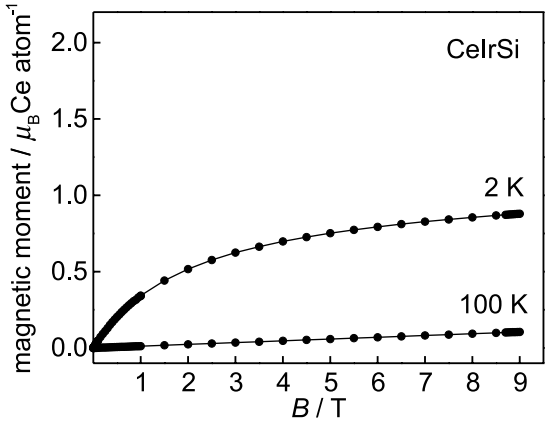

Fig. 8. Magnetization *vs.* external flux density for CeIrSi at 2 and 100 K

Acknowledgements

We thank *H.-J. Göcke* for the work at the scanning electron microscope and the Degussa-Hüls AG for a generous gift of iridium powder. This work was financially supported by the Deutsche Forschungsgemeinschaft. *R. M.* and *M. V.* are indebted to the Alexander von Humboldt Foundation for research stipends.

References

[1] Parthé E, Chabot B (1984) Crystal Structures and Crystal Chemistry of Ternary Rare Earth-Transition Metal Borides, Silicides and Homologues. In: Gschneidner KA Jr, Eyring L (1984) Handbook on the Physics and Chemistry of Rare Earths, chapt 48. Elsevier, Amsterdam
[2] Rogl P (1984) Phase Equilibria in Ternary and Higher Order Systems with Rare Earth Elements and Silicon. In: Gschneidner KA Jr, Eyring L, Handbook on the Physics and Chemistry of Rare Earths, chapt 51. Elsevier, Amsterdam
[3] Salamakha PS, Sologub OL, Bodak OI (1999) Ternary Rare-Earth–Germanium Systems. In: Gschneidner KA Jr, Eyring L, Handbook on the Physics and Chemistry of Rare Earths, chapt 173. Elsevier, Amsterdam
[4] Salamakha PS (1999) Crystal Structures and Crystal Chemistry of Ternary Rare-Earth Germanides. In: Gschneidner KA Jr, Eyring L, Handbook on the Physics and Chemistry of Rare Earths, chapt 174. Elsevier, Amsterdam
[5] Szytuła A, Leciejewicz J (1994) Handbook of Crystal Structures and Magnetic Properties of Rare Earth Intermetallics. CRC Press, Boca Raton, Florida
[6] Emsley J (1999) The Elements. Oxford University Press, Oxford
[7] Hovestreydt E, Engel N, Klepp K, Chabot B, Parthé E (1982) J Less-Common Met **85**: 247
[8] Klepp K, Parthé E (1982) Acta Crystallogr B **38**: 1541
[9] Chevalier B, Lejay P, Cole A, Vlasse M, Etourneau J (1982) Solid State Commun **41**: 801
[10] Wang X-Z, Chevalier B, Etourneau J, Hagenmuller P (1985) Mater Res Bull **20**: 517
[11] Islam MS (1987) J Bangladesh Acad Sci **11**: 15
[12] Penc B, Baran S, Hofmann M, Leciejewicz J, Szytuła A (2000) Physica B **276–278**: 620
[13] Mishra R, Hoffmann R-D, Pöttgen R (2001) Z Anorg Allg Chem **627**: 1787
[14] Szytuła A, Hofmann M, Leciejewicz J, Penc B, Zygmunt A (2001) J Alloys Compd **316**: 58
[15] Pöttgen R, Gulden Th, Simon A (1999) GIT Labor Fachzeitschrift **43**: 133
[16] Niepmann D, Prots' YuM, Pöttgen R, Jeitschko W (2000) J Solid State Chem **154**: 329
[17] Yvon K, Jeitschko W, Parthé E (1977) J Appl Crystallogr **10**: 73
[18] Sheldrick GM (1997) SHELXS-97, Program for the Solution of Crystal Structures, University of Göttingen
[19] Sheldrick GM (1997) SHELXL-97, Program for Crystal Structure Refinement, University of Göttingen
[20] Flack HD, Bernadinelli G (1999) Acta Crystallogr A **55**: 908
[21] Flack HD, Bernadinelli G (2000) J Appl Crystallogr **33**: 1143
[22] Roisnel T, Rodríguez-Carvajal J (2001) Fullprof.2k V. 2.0, Laboratoire Léon Brillouin (CEA-CNRS), 91191 Gif-sur-Yvette Cedex (France)
[23] Bérar JF, Lelann P (1991) J Appl Crystallogr **24**: 1
[24] Lueken H (1999) Magnetochemie. Teubner, Stuttgart
[25] Galadzhun YaV, Hoffmann R-D, Pöttgen R, Adam M (1999) J Solid State Chem **148**: 425
[26] Niepmann D, Pöttgen R, Künnen B, Kotzyba G, Mosel BD (2000) Chem Mater **12**: 533
[27] Johrendt D, Kotzyba G, Trill H, Mosel BD, Eckert H, Fickenscher Th, Pöttgen R (2002) J Solid State Chem **164**: 201
[28] Shoemaker CB, Shoemaker DP (1965) Acta Crystallogr **18**: 900
[29] Mishra R, Pöttgen R, Kotzyba G (2001) Z Naturforsch **56b**: 463

[30] Hovestreydt E (1988) J Less-Common Met **143**: 25
[31] Niepmann D, Pöttgen R (2001) Intermetallics **9**: 313
[32] Verniere A, Lejay P, Bordet P, Chenavas J, Tholence JL, Boucherle JX, Keller N (1995) J Alloys Compd **218**: 197
[33] Donohue J (1974) The Structures of the Elements. Wiley, New York
[34] Klepp K, Parthé E (1982) Acta Crystallogr B **38**: 1105
[35] Brauer G, Haag H (1952) Z Anorg Allg Chem **267**: 198
[36] Albering JH, Pöttgen R, Jeitschko W, Hoffmann R-D, Chevalier B, Etourneau J (1994) J Alloys Compd **206**: 133